Mechanistic studies of the water oxidation reaction with molecular iron catalysts

D'Agostini, S.

Chapter 3

Investigation of the equilibrium between the monomeric and dimeric forms of the Fe(bbpya)-based water oxidation catalysts

In this chapter the molecular water oxidation catalysts [{Fe(Hbbpya)(MeOH)}$_2$(μ-O)](OTf)$_4$ (Hbbpya = N,N-bis(2,2'-bipyrid-6-yl)amine) and [{Fe(Mebbpya)(H$_2$O)}$_2$(μ-O)](OTf)$_4$ were investigated. An equilibrium between the dimeric and the monomeric form of the catalysts was identified, with the monomeric form generated during catalysis being the active species responsible for water oxidation. In case of [{Fe(Hbbpya)(MeOH)}$_2$(μ-O)](OTf)$_4$ a water nucleophilic attack mechanism was proposed, confirmed by a kinetic isotope effect value of 1.6. In presence of [{Fe(Mebbpya)(H$_2$O)}$_2$(μ-O)](OTf)$_4$ the KIE value of 0.9 suggests that a different rate-determining step is involved. An electron transfer process or a bimolecular pathway were suggested as possible mechanisms of action.

The results presented in this chapter are to be submitted for publication: S. D'Agostini, J.F. Louwen, M.A. Siegler and D.G.H. Hetterscheid.

3.1 Introduction

In the field of water oxidation catalysis performed with homogeneous catalysts based on first-row transition metals several examples of dinuclear oxygen-bridged iron complexes have been reported (Fig. 3.1).[1-4] In many cases an equilibrium between monomeric and dimeric iron(III) species has been observed, with the catalysts exhibiting activity both in their monomeric and dimeric form. For complex **1** reported by Parent *et al.* an equilibrium between monomeric and dimeric forms of the catalyst was established.[1] The iron(III) μ-oxo dimer was identified as the active species during the initial phase of water oxidation. The catalyst showed complex kinetic behaviour due to the formation of additional species identified as an Fe^{IV} monomer and an $Fe^{III}Fe^{IV}$ dimer. Both forms showed catalytic activity in presence of sodium periodate, with the monomeric form being favoured under acidic conditions and showing higher catalytic rates. Complex **2**

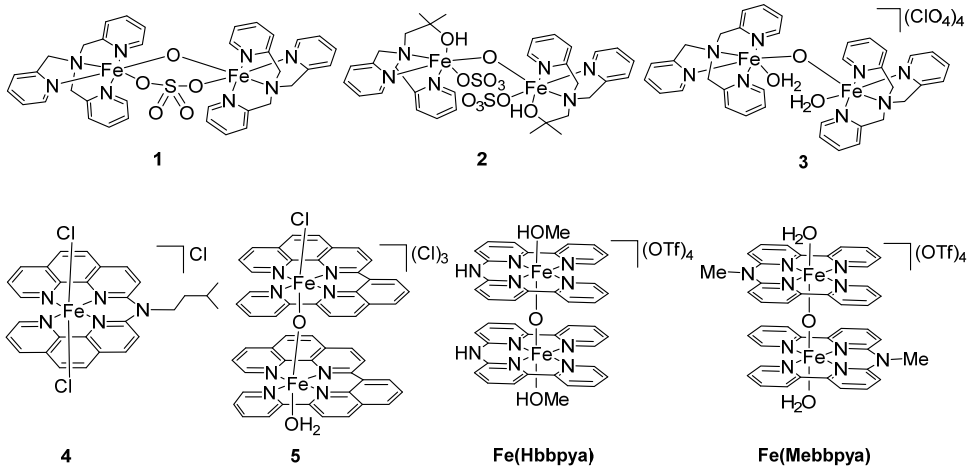

Figure 3.1. Structures of the complexes evaluated in this study.

also reported by Parent *et al.* proved to be active towards the water oxidation reaction, both in its mononuclear and dinuclear form, showing higher catalytic activity in its mononuclear form.[1] Upon increasing the catalyst concentration formation of Fe^{IV} dimers and deactivation of the catalyst were observed, from which it was concluded that the dimers that are formed are not catalytically active. The group of Thummel developed mononuclear and dinuclear iron complexes of square planar tetradentate polypyridyl-type ligands.[2] In presence of large excess of cerium ammonium nitrate (CAN) the μ-oxo-bridged dimer **5** showed high catalytic activity in water oxidation with turnover frequency (TOF)

values up to 2.2 s^{-1}. The mononuclear complex **4** showed lower activity, with TOFs of 0.23 s^{-1}. It was suggested that the steric encumbrance of the N-isopentyl group of **4** may inhibit the formation of the dimer. Najafpour *et al.* reported the dimeric complex **3** as an efficient catalyst for the water oxidation reaction.[3]

Both monomeric and dimeric complexes can serve as precursors for catalysts for the oxygen evolution reaction (OER), yet it is unclear whether the dimers or monomers are the active species. Catalyst concentration, pH and steric effects can affect the prevalence of one structure over the other and as a result affect the related catalytic activity.

In our group we developed the dinuclear oxo-bridged iron complex $[\{Fe(Hbbpya)(MeOH)\}_2(\mu\text{-}O)](OTf)_4$ (Hbbpya = N,N-bis(2,2'-bipyrid-6-yl)amine).[4] In order to move away from the use of chemical oxidants, the complex was investigated electrochemically and was reported to be an active molecular electrocatalyst for the water oxidation reaction, showing a significantly lower overpotential in presence of graphitic electrodes, compared to other electrode materials.[4] From these preliminary electrochemical studies it was proposed that an equilibrium between the dimeric and monomeric forms of the catalyst takes place. Therefore the main research question of the present work concerns the identification of the nature of the active species and the determination of the catalytic mechanism.

Monomeric water oxidation catalysts often react *via* a water nucleophilic attack (WNA) mechanism (Fig. 3.2).[5] In this type of mechanism the O−O bond formation step involves a high-energy transition state. When the formation of the O−O bond is rate-determining the facilitation of this step can lead to an improvement of the catalytic performance. The energy barrier associated with the O−O bond formation step can be lowered by the presence of proton shuttles, which activate the incoming water molecule by abstracting a proton, thereby avoiding the formation of the energetically unfavourable intermediate.[5]

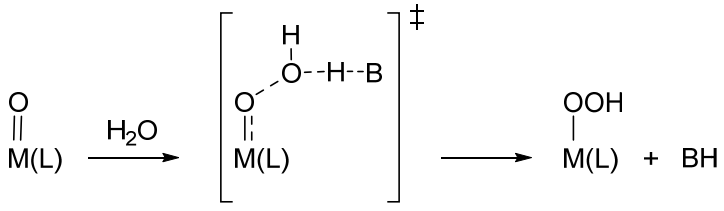

Figure 3.2. Schematic representation of a water nucleophilic attack mechanism involving the proton acceptor B (M = metal, L = ligand).

Previous studies performed by Meyer *et al.* on the water oxidation catalyst $[Ru(Mebimpy)(bpy)(OH_2)]^{2+}$ (Mebimpy = 2,6-bis(1-methylbenzimidazol-2-yl)pyridine; bpy = 2,2'-bipyridine) showed that added bases can act as proton acceptors, accelerating the O−O bond formation by concerted atom-proton-transfer (APT).[5] In case of $[\{Fe(Hbbpya)(MeOH)\}_2(\mu\text{-}O)](OTf)_4$ the amine present in the structure of the complex in a deprotonated form may act as proton shuttle to activate a water molecule. When the O−H bond is broken during the rate-determining step (rds) of the reaction a kinetic isotope effect (KIE) is expected, with a lower reaction rate in deuterium oxide than in water, which leads to a KIE > 1. Meyer *et al.* reported an increase in KIE with decreasing base strength through a series of bases from water (KIE = 6.6) to HPO_4^{2-} (KIE = 2.3) in a base-catalysed APT process.[5]

Llobet *et al.* have shown that incorporation of a proton shuttle in the ligand framework can facilitate APT leading to very high turnover frequencies for a ruthenium-based water oxidation catalyst (TOF = 8000 s^{-1} at pH 7 and 50000 s^{-1} at pH 10).[6] Given that the pK_a of the amine group in the ligand Hbbpya was found between 5 and 9,[7-8] it is likely that this ligand moiety is involved in proton shuttling during APT and/or proton-coupled electron transfer (PCET) steps. In this study we further investigated this hypothesis, by removal of the N−H functionality by methylation. The synthesis and characterization of the new complex $[\{Fe(Mebbpya)(H_2O)\}_2(\mu\text{-}O)](OTf)_4$ is described, as well as its activity in electrocatalytic water oxidation. For simplicity the notation Fe(Hbbpya) and Fe(Mebbpya) will be used in this chapter for $[\{Fe(Hbbpya)(MeOH)\}_2(\mu\text{-}O)](OTf)_4$ and $[\{Fe(Mebbpya)(H_2O)\}_2(\mu\text{-}O)](OTf)_4$, respectively.

3.2 Results and discussion

3.2.1 Synthesis and characterization of Fe(Mebbpya)

The Hbbpya ligand was methylated using methyl iodide after deprotonation with KOtBu. Fe(Mebbpya) was synthesized by adding 1 equivalent of $Fe(OTf)_2 \cdot 5.5\ H_2O$ in degassed methanol to the Mebbpya ligand (Scheme 3.1). Dark brown crystals of the complex were obtained by slow vapour diffusion of Et_2O into a concentrated methanolic solution of the crude product. Fe(Mebbpya) was characterized by mass spectrometry, elemental analysis and X-ray crystallography.

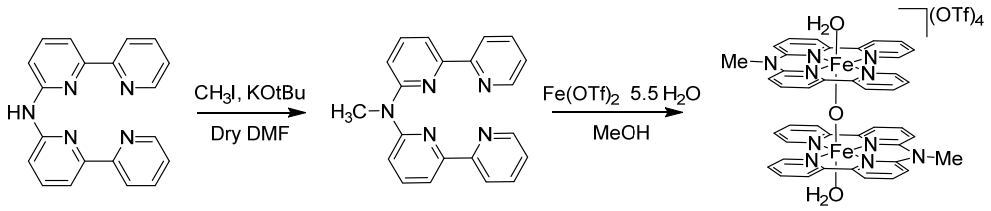

Scheme 3.1. Synthetic route of Fe(Mebbpya).

As shown in Figure 3.3b, Fe(Mebbpya) consists of two iron sites bridged by an oxo ligand. Each iron site holds an axial water, an oxo ligand and the tetradentate Mebbpya ligand in the equatorial plane in a distorted octahedral geometry. The bond distances and angles are very similar for both iron sites within the unit cell (Table A2, Appendix A). The bond distances for all eight Fe–N bonds fall into the range of 2.11 to 2.14 Å. The N−Fe−N angles of the five-membered chelate rings fall in the range of 77.9° to 78.3° and the N−Fe−N bond angles of the six-membered chelate rings account for 86.5° and 86.7°, which is close to the ideal 90° of a square-planar geometry, while the open N−Fe−N bond angles are much wider at 117.0° and 114.4°. The bond distances between the iron centres and the bridging oxo ligand are 1.77 and 1.80 Å, which are shorter than the Fe−O bonds distances from the water ligands, accounting for 2.10 and 2.18 Å. The bond distance between the nitrogen and the methyl group is for both bonds 1.48 Å. Both methyl groups are oriented downwards with respect to the water ligand. The Mebbpya ligands are fairly planar with internal torsion angles of 1.0° and 1.3° and are such oriented that the methyl groups are on the opposite side with respect to each other.

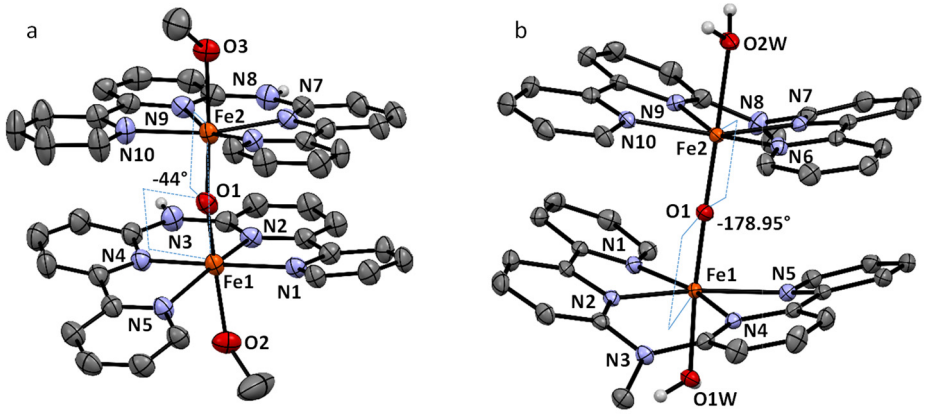

Figure 3.3. X-ray crystal structures of (a) Fe(Hbbpya)[4] and (b) Fe(Mebbpya) showing ellipsoids at 50% probability at 110(2) K. For clarity the hydrogen atoms, the four triflate counter-ions, one lattice methanol and one lattice water solvent molecules are omitted.

When comparing the dinuclear Fe(Mebbpya) and Fe(Hbbpya) complexes the Fe−N bond distances and bond angles show virtually identical values (Table A2, Appendix A). Remarkable differences are observed in the Fe−O−Fe bond angles, measured at 174.9° for Fe(Mebbpya), which is close to the expected 180° and significantly larger than the Fe−O−Fe bond angle in Fe(Hbbpya) (155.8°). Moreover, while in Fe(Hbbpya) the two Hbbpya ligands are not aligned directly on top of each other, with a rotation around the Fe1−Fe2 axis of 44°, the Mebbpya ligands in Fe(Mebbpya) show alignment, with a torsion angle of 179°. The Mebbpya ligand exhibits a butterfly configuration, whereas the Hbbpya ligand shows a helical configuration. The differences in Fe−O−Fe angles and torsion angles between the two complexes are likely caused by packing effects within the single crystal.

3.2.2 Stability of Fe(Mebbpya) in aqueous solutions

UV-vis measurements of aqueous solutions of Fe(Mebbpya) were performed to check the stability of the dimeric species over time. UV-vis spectra were recorded every 15 minutes for 7.5 hours at a concentration of 10 µM of the dinuclear complex (Fig. 3.4a). Changes were observed over time, resulting in the decrease

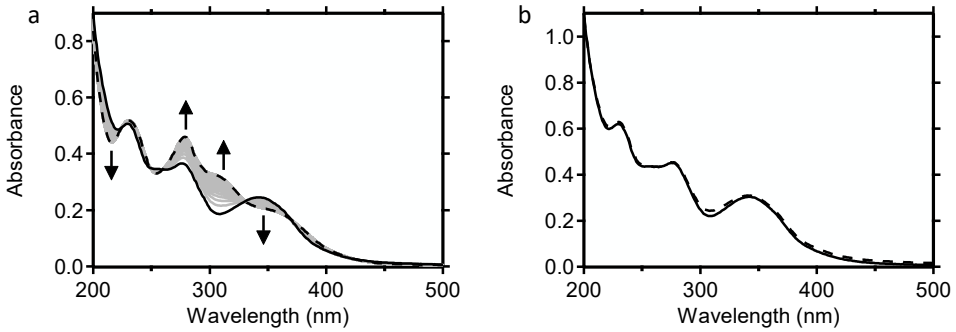

Figure 3.4. (a) Evolution of the UV-vis absorption of 10 µM Fe(Mebbpya) in water over 7.5 h, recorded in intervals of 15 minutes. The first scan (t = 0, solid line) and last scan (t = 450 min, dashed line) are displayed in black and the intermediate scans are displayed in grey. The arrows indicate the change observed over time. (b) Evolution of the UV-vis absorption of 1 mM Fe(Mebbpya) in water over 7.5 h, recorded in intervals of 15 minutes. Displayed are the first scan (solid line) and last scan (dashed line). The 1 mM complex solution was diluted to 10 µM prior to the UV-vis measurement.

and increase of the absorption bands at 350 nm and 277 nm, respectively, together with the appearance of a shoulder around 360 nm. The absorption band at 350 nm is associated to the Fe−O−Fe interaction of the µ-oxo dimer[2] and its

decrease over time points to the formation of a monomer. The monomer-dimer kinetics appeared to be very slow. The same experiment was repeated at a concentration of 1 mM in order to check the structure of the complex in aqueous solutions at realistic catalytic conditions. Taking advantage of the slow monomer-dimer kinetics, the solution was quickly diluted to 10 µM only prior to the UV-vis measurement to avoid overload of the UV-vis signal (Fig. 3.4b). In this case no significant changes were observed over time, suggesting the prevalence of the dimer form in these more concentrated conditions.

3.2.3 Electrochemical investigation of Fe(Hbbpya) and Fe(Mebbpya)

3.2.3a Effects of the electrode material

Previous studies performed in our group showed that Fe(Hbbpya) is an active molecular electrocatalyst for the water oxidation reaction.[4] Remarkable effects of the electrode material on the performance of the catalyst were observed. In particular a significantly lower catalytic overpotential was observed on graphitic electrodes in comparison to other electrode materials. Therefore the interaction of Fe(Mebbpya) with different electrode materials was evaluated as well. Besides the glassy-carbon electrode (GC) used in most of the experiments, the other working electrodes that were tested were a boron-doped-diamond disk (BDD), a pyrolytic graphite disk (PG), a gold disk and an indium-tin-oxide plate (ITO). Cyclic voltammograms (CV) of a 0.5 mM solution of the dinuclear complex Fe(Mebbpya) in 0.1 M Na_2SO_4 were recorded by scanning the potential between 0.0 and 2.0 V vs. RHE, at a scan rate of 100 mV/s (Fig. 3.5). The results obtained with the BDD and the PG working electrodes are qualitatively similar to the ones obtained with the GC electrode (Fig. 3.6a), aside from higher catalytic currents which are due to the larger surface area of the BDD and PG disks compared to the GC rod that was used. The electrochemistry of Fe(Mebbpya) using gold and ITO working electrodes appeared to be significantly more complex due to the oxidation of the gold surface and the slow electron-transfer kinetics observed at ITO, respectively. For these reasons it was decided not to use these electrodes in further experiments. In contrast to Fe(Hbbpya), no apparent effect of the electrode material on the onset of the catalytic current is observed in case of Fe(Mebbpya).

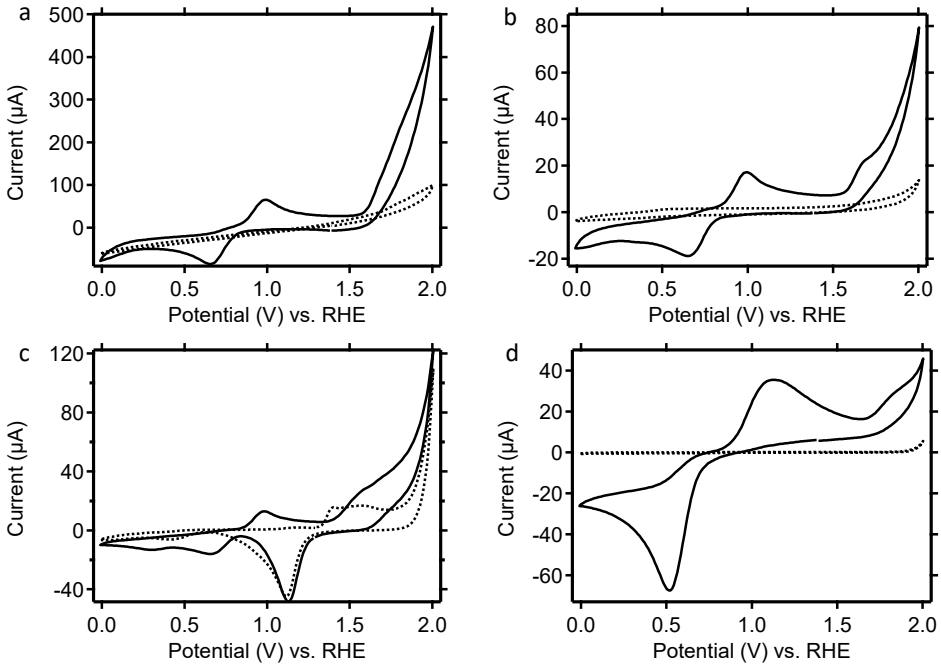

Figure 3.5. Cyclic voltammograms of 0.5 mM Fe(Mebbpya) in 0.1 M Na_2SO_4 using different working electrodes, at a scan rate of 100 mV/s. Displayed are the second scans for Fe(Mebbpya) (solid line) and the respective blank (dotted line) measured with (a) BDD, (b) PG, (c) gold and (d) ITO working electrodes.

3.2.3b Electrochemical investigation

Before investigating the new complex Fe(Mebbpya) we reproduced the results previously obtained in our group with Fe(Hbbpya), which showed peculiar electrochemical features.[9] As shown in Figure 3.6a, the first scan of a cyclic voltammogram of the complex recorded with a GC working electrode shows two oxidation and two reduction events, which were tentatively assigned to the $[Fe^{II}Fe^{II}]/[Fe^{II}Fe^{III}]$ and $[Fe^{II}Fe^{III}]/[Fe^{III}Fe^{III}]$ transitions. In the second scan recorded after the catalyst has been exposed to high potentials (2.0 V vs. RHE) only one oxidation and one reduction waves are visible, with a large peak separation of 453 mV. Subsequently, 50 scans were recorded between 0.0 and 1.4 V (Fig. 3.6b) and over time the original four redox events observed in the first scan of the first cyclic voltammogram (Fig. 3.6a) were restored. The change in redox behaviour after exposure to high potentials points to a structural change of the catalyst, which reverts over time. However, this apparent reversion to the original double

redox wave may also be caused by diffusion of unreacted starting material to the electrode in the course of the experiment.

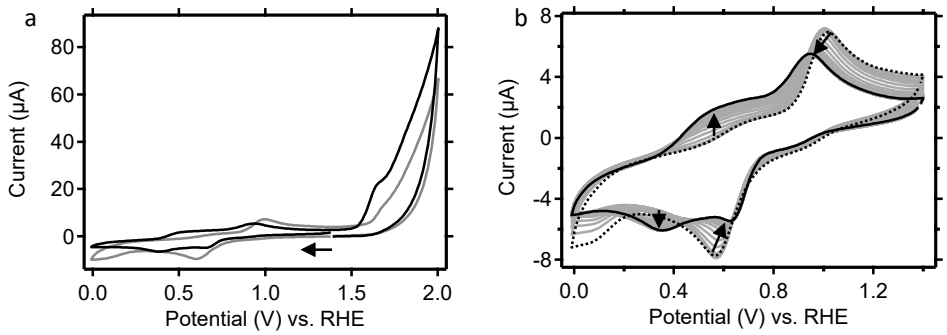

Figure 3.6. Cyclic voltammograms of 0.5 mM Fe(Hbbpya) in 0.1 M Na_2SO_4, at a scan rate of 100 mV/s, using a GC working electrode. (a) First scan (black line) and second scan (grey line) between 0.0 and 2.0 V vs. RHE, starting at 1.4 V vs. RHE. The arrow indicates the initial direction of the scan. (b) Demonstration of the evolution over time of the redox events after initially scanning to 2.0 V vs. RHE. Shown are 50 cycles between 0.0 and 1.4 V vs. RHE, starting at 1.4 V vs. RHE. The second scan (dotted line) and the last scan (solid line) are displayed in black while the intermediate scans are displayed in grey. The arrows indicate the change observed over time.

Contrary to Fe(Hbbpya), its methylated version shows the presence of single oxidation and reduction waves with a large peak separation (ΔE = 200 mV), both in the first and in the second scan of a voltammetry experiment with an upper vertex potential of 2.0 V versus RHE. However, the peak potentials do shift by +30 mV between the oxidation events of the first and second scan (Fig. 3.7a).

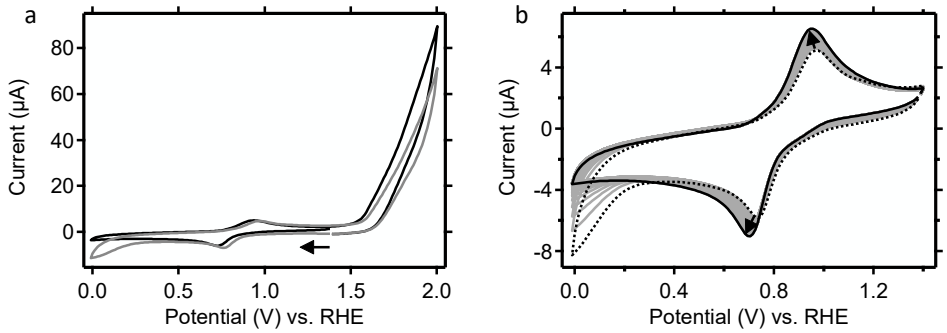

Figure 3.7. Cyclic voltammograms of 0.5 mM Fe(Mebbpya) in 0.1 M Na_2SO_4, at a scan rate of 100 mV/s, using a GC working electrode. (a) First scan (black line) and second scan (grey line), cycled between 0.0 and 2.0 V vs. RHE, starting at 1.4 V vs. RHE. The arrow indicates the starting direction of the scan. (b) Demonstration of the evolution over time of the redox events after initially scanning to 2.0 V vs. RHE. Shown are 50 cycles between 0.0 and 1.4 V vs. RHE, starting at 1.4 V vs. RHE. The second scan (dotted line) and the last scan (solid line) are displayed in black while the intermediate scans are displayed in grey. The arrows indicate the change observed over time.

Although a single redox event is observed, this may still correspond to an overall two-electron $[Fe^{III}Fe^{III}]/[Fe^{II}Fe^{II}]$ transition. Immediately afterwards the voltammetry experiment between 0.0 and 2.0 V, 50 scans were recorded between 0.0 and 1.4 V (Fig. 3.7b) and over time the original peaks observed in the first scan of the first cyclic voltammogram (Fig. 3.7a) were restored.

Further investigation of the redox events for both complexes was performed with Differential Pulse Voltammetry (DPV) (Fig. 3.8). In DPV experiments the contribution from background currents is reduced, which allows to observe the redox events that are less pronounced with cyclic voltammetry and to enhance the reversible ones. A more detailed description of the DPV experiments is reported in Chapter 2 of this thesis.[10] The reversible redox couple between 0.5 V and 1.0 V is visible for both complexes. The oxidation event observed in the cyclic voltammogram of Fe(Hbbpya) around 1.6 V, but which is absent for Fe(Mebbpya), is now visible in the DPV of both complexes. The DPV experiment of Fe(Mebbpya) shows a reduction event around 1.7 V (Fig. 3.8b), which is weaker in the DPV of Fe(Hbbpya) (Fig. 3.8a). It appears that the Mebbpya complex is more difficult to oxidize than the Hbbpya complex, despite the more electron-donating capacity of the methyl group. Most likely this is caused by better delocalization of spin density in the π-conjugated system of the deprotonated bbpya ligand.

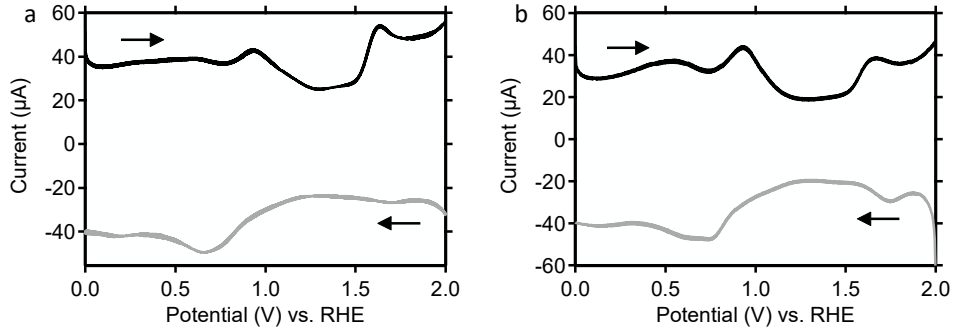

Figure 3.8. Results of forward (black line) and backward (grey line) scans of DPV experiments of (a) 0.5 mM Fe(Hbbpya) and (b) 0.5 mM Fe(Mebbpya), performed in 0.1 M Na_2SO_4, using a GC working electrode. The arrows indicate the direction of the scan. The values of the DPV settings used during the experiments were 0.05 V for the modulation amplitude, 0.003 s for the modulation time and 0.005 s for the interval time.

When comparing the catalytic waves (Fig. 3.9), it appears that both complexes show virtually the same catalytic activity and onset potentials for the water oxidation reaction around 1.6 V on a graphitic electrode. Fe(Hbbpya) shows an

extra oxidation event around 1.6 V in the first scan which is somewhat less pronounced in the second scan and absent in case of Fe(Mebbpya) in both scans. The values of the catalytic currents (i_{cat}) at 2.0 V vs. RHE of both catalysts were compared at 0.5 mM concentrations, calculated from the dimer. The values were taken from the first and the second scan of the CV experiments. In the first scan i_{cat} values around 90 µA were obtained both for Fe(Hbbpya) and Fe(Mebbpya), while in the second scans a lower activity was found for both complexes, with i_{cat} values around 70 µA.

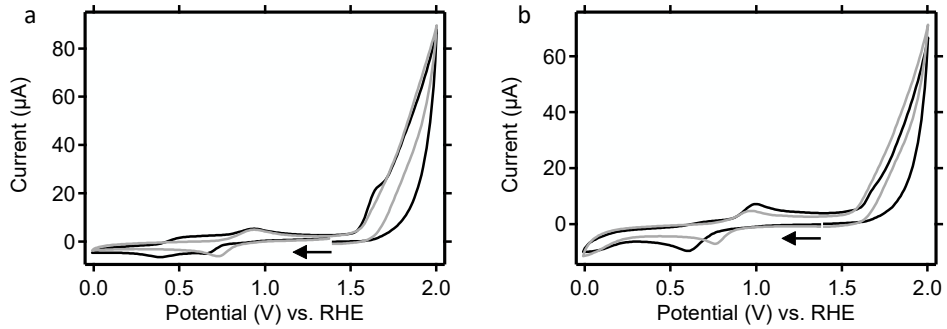

Figure 3.9. (a) Cyclic voltammograms of 0.5 mM Fe(Hbbpya) (black line) and Fe(Mebbpya) (grey line) in 0.1 M Na_2SO_4, at a scan rate of 100 mV/s, using a GC working electrode. Displayed are the first scans for both complexes, scanning between 0.0 and 2.0 V vs. RHE, starting at 1.4 V vs. RHE. (b) Cyclic voltammograms of 0.5 mM Fe(Hbbpya) (black line) and Fe(Mebbpya) (grey line) in 0.1 M Na_2SO_4, at a scan rate of 100 mV/s, using a GC working electrode. Displayed are the second scans for both complexes, scanning between 0.0 and 2.0 V vs. RHE, starting at 1.4 V vs. RHE. The arrows indicate the direction of the scan.

3.2.3c Spectroelectrochemical investigation

The recovery of the original signals observed in the cyclic voltammograms of Fe(Hbbpya) and Fe(Mebbpya) after repeated scanning at potentials lower than the onset potential for water oxidation (Fig. 3.6b and Fig. 3.7b) can be a consequence of a slow setting equilibrium between a dimeric and monomeric form of the complexes. However, it may also be caused by diffusion of unreacted pre-catalyst to the electrode surface. In order to rule this out, bulk electrolysis was performed in combination with spectroscopy in an Optically Transparent Thin-Layer Electrochemical cell (OTTLE cell). The OTTLE cell allows one to observe the structural changes of the complex during catalysis by combining electrochemistry with *in situ* UV-vis spectroscopy. Given the features of the OTTLE cell device, where the electrodes are placed between two CaF_2 windows which adhere to each other, a volume of only 200 µL of solution is needed to fill the cell.

In this way the effects of diffusion of the solution to and from the electrode surface can be excluded and a complete conversion is achieved, leaving no unreacted starting material.

Fe(Hbbpya) was investigated by recording a UV-vis spectrum before bulk electrolysis. Figure 3.10a (black line) shows the absorption band at 350 nm, characteristic of the μ–O bridge present in the catalyst dimeric form.[2]

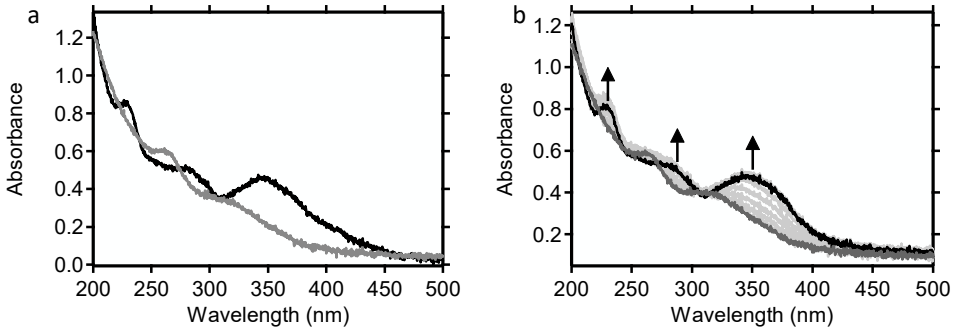

Figure 3.10. Results of the spectroelectrochemical experiments of 1.0 mM Fe(Hbbpya) in 0.1 M Na_2SO_4 in an OTTLE cell. (a) UV-vis spectrum of Fe(Hbbpya) recorded before (black line) and after applying 2.0 V vs. RHE for 12 minutes (grey line). (b) Demonstration of the evolution of the complex over time. After applying 2.0 V vs. RHE for 12 minutes no potential was applied for 56 minutes and the solution was monitored every 4 minutes. Depicted are the first scan (dark grey line, t = 4 min), the last scan (black line, t = 56 min) and the intermediate scans corresponding to UV-vis spectra taken every 4 minutes. The arrows indicate the change observed over time.

Subsequently a catalytic potential of 1.2 V vs. a silver pseudo-reference electrode, which corresponds to a value of 2.0 V vs. RHE (see Experimental section), was applied for 12 minutes and a UV-vis spectrum was recorded afterwards. As shown in Figure 3.10a (grey line) the absorption band at 350 nm disappeared, suggesting that the compound directly after catalysis is a monomer, in which no μ–O bridge is present. After exposure to the catalytic potential for 12 minutes the solution was left to stand and a UV-vis spectrum was recorded every 4 minutes for 56 minutes to monitor the evolution of the system over time. After 56 minutes the original band at 350 nm was restored (Fig. 3.10b). When comparing the results obtained from the cyclic voltammograms (Fig. 3.6) and from the OTTLE cell (Fig. 3.10) a correlation can be found. In both experiments after catalysis a change is observed, which translates in the disappearance of the band at 350 nm in the UV-vis spectra (Fig. 3.10a) and in the presence of only one oxidation and one reduction events in the voltammograms (Fig. 3.6a). Over time (56 min for the UV-vis and 50 scans for the CV) both the band at 350 nm and the original four

redox events are fully restored (Fig. 3.10b and Fig. 3.6b). The disappearance of the band at 350 nm associated to the μ-oxo dimer points to a conversion of a dimeric to a monomeric form of the complex. The same observation is valid for the electrochemical experiments, which showed four redox events before and one oxidation and one reduction waves after catalysis, which may be related to a dimeric and a monomeric form of the catalyst.

In the same manner as for Fe(Hbbpya), its methylated version Fe(Mebbpya) was investigated by spectroelectrochemistry (Fig. 3.11). During the experiments performed with the OTTLE cell a disappearance and restoration of a band at 350 nm was observed for Fe(Mebbpya) as well. Additionally a new band at 311 nm appeared after catalysis which decreased over time. However, in case of Fe(Mebbpya) the spectroscopic changes (Fig. 3.11) showed to be more pronounced than the changes in the cyclic voltammograms (Fig. 3.7). These results clearly show that for both complexes the same monomer-dimer conversion reactions are taking place.

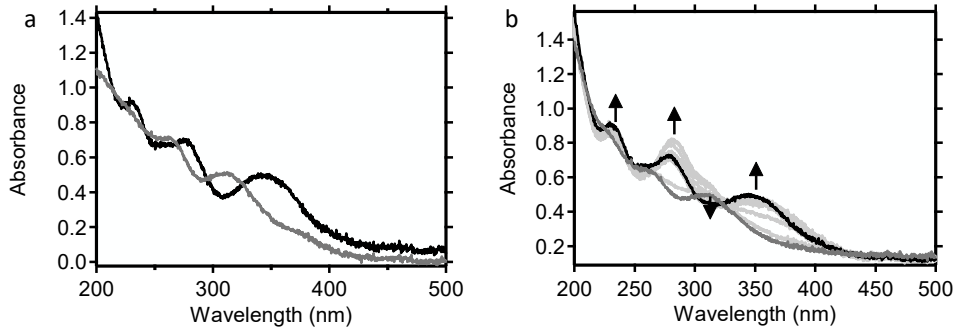

Figure 3.11. Results of the OTTLE cell experiments of 1.0 mM Fe(Mebbpya) in 0.1 M Na_2SO_4. (a) UV-vis spectrum of Fe(Mebbpya) recorded before (black line) and after applying a 2.0 V vs. RHE for 12 minutes (grey line). (b) Demonstration of the evolution of the complex over time. After applying 2.0 V vs. RHE for 12 minutes no potential was applied for 56 minutes and the solution was monitored every 4 minutes. Depicted are the first scan (dark grey line, t = 4 min), the last scan (black line, t = 56 min) and the intermediate scans corresponding to UV-vis spectra taken every 4 minutes. The arrows indicate the change observed over time.

3.2.3d Electrochemical Quartz Crystal Microbalance studies (EQCM)

Since Fe_2O_3 is a known catalyst for water oxidation, it is important to establish that deposits of Fe_2O_3 are not being formed on the working electrode, which then may be responsible for (part of) the observed reactivity. To rule out the formation of catalytically active surface deposits, electrochemical quartz crystal

microbalance (EQCM) experiments were carried out.[11-14] In EQCM experiments the working electrode consists of a thin layer of gold, deposited on a quartz crystal which is oscillated during the electrochemical experiment. Changes in oscillation frequency can be directly related to changes in mass of the electrode.[15] A decrease in frequency corresponds to an increase in mass, as a consequence of a deposition of catalytic material on the electrode surface. In order to avoid the mass change associated with gold oxide formation and reduction, the gold surface was oxidized before the EQCM measurement and the potential was kept above 1.3 V during each experiment. The results obtained with Fe(Hbbpya) show no significant change in the mass of the electrode when compared to the experiment conducted in presence of $Fe(OTf)_2$.[4] In case of equal concentrations in [Fe] (0.5 mM for the dinuclear complex Fe(Hbbpya) and 1.0 mM for $Fe(OTf)_2$), a clear decrease in vibration frequency of 100 Hz was observed, related to the formation of a deposit on the electrode surface. No mass deposition of complex on the working electrode was observed for Fe(Mebbpya) as well, as shown in Figure 3.12 (top). In addition usage of $Fe(OTf)_2$ resulted in catalytic activity with a later onset for water oxidation when compared to the Febbpya systems, also in presence of a PG working electrode.[4]

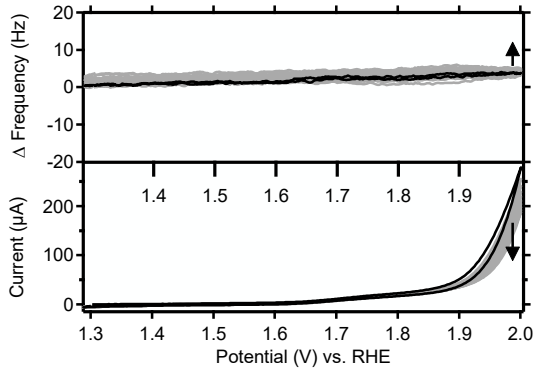

Figure 3.12. Cyclic voltammetry in combination with QCM of 0.5 mM Fe(Mebbpya) in 0.1 M Na_2SO_4 at a scan rate of 100 mV/s, using a gold working electrode. Shown are scan 1 (black) and scans 2 to 10 (grey) of the cyclic voltammogram experiment (bottom) and the corresponding change in resonance frequency (top). The arrows indicate the change observed over time.

3.2.3e On-line Electrochemical Mass Spectrometry studies (OLEMS)

In order to assess the product formation during a potential sweep in the presence of Fe(Mebbpya) on-line electrochemical mass spectrometry (OLEMS) experiments were performed in combination with cyclic voltammetry. In the OLEMS

measurements the *m/z* traces of selected gaseous products, sampled in close proximity to the electrode surface, are recorded as a function of the applied potential.[16] During all OLEMS experiments dioxygen evolution was monitored by recording the *m/z* = 32 together with *m/z* = 44 to monitor any CO_2 formation caused by potential ligand decomposition.[17-20]

In the OLEMS experiment recorded with a PG working electrode (Fig. 3.13a) Fe(Mebbpya) shows water oxidation activity. In the current trace (Fig. 3.13a,

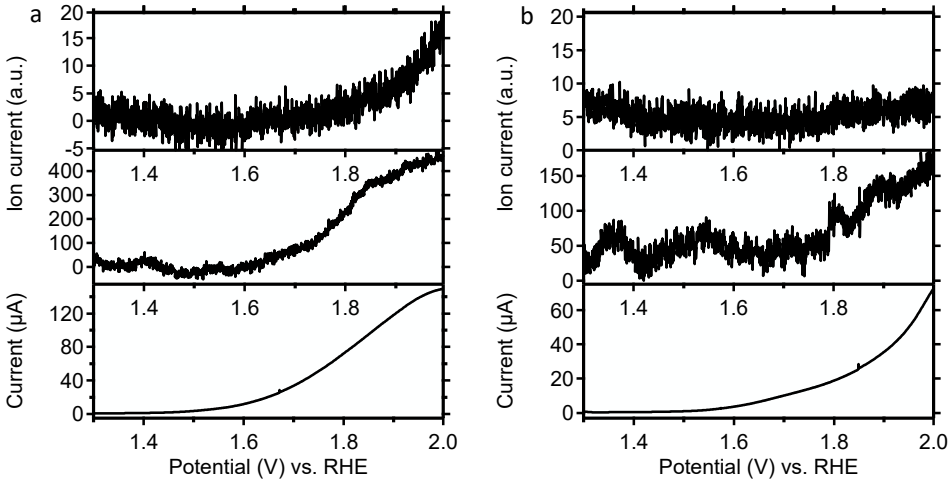

Figure 3.13. Cyclic voltammetry in combination with OLEMS of 0.5 mM Fe(Mebbpya) in 0.1 M Na_2SO_4 at a scan rate of 1 mV/s. Depicted are the *m/z* traces of CO_2 (top), O_2 (middle) and the corresponding current (bottom). (a) Experiment performed using a PG working electrode. The CO_2 trace was zoomed of a factor of 20 compared to the O_2 trace range. (b) Experiment performed using a gold working electrode. The CO_2 trace was zoomed of a factor of 7.5 compared to the O_2 trace range. For the sake of clarity only the forward sweep of the 1st scan is shown.

bottom) an oxidative current can be observed starting at 1.6 V with a sharp increase around 1.8 V. The mass trace for O_2 (Fig. 3.13a, middle) correlates with the current profile and shows an onset for dioxygen evolution at about 1.6 V. As shown in the CO_2 trace (Fig. 3.13a, top) a small amount of CO_2 was formed. In order to verify whether the carbon dioxide produced originated from decomposition of the ligand or from the electrode material, OLEMS experiments of Fe(Mebbpya) were performed with a gold working electrode. As shown in Figure 3.13b no CO_2 formation was observed, which indicates that the CO_2 formation observed in presence of a PG working electrode most likely originates from the electrode material itself and not from ligand decomposition. Moreover, CO_2 formation was detected in OLEMS experiments with a PG working electrode

both in presence and in absence of metal complexes in solution (see Chapter 5 of this thesis).

Dioxygen formation was previously detected with OLEMS using Fe(Hbbpya) as reported by Kottrup,[4,9] but some differences are observed when the results are compared to those of Fe(Mebbpya). The recorded current (Fig. 3.14a, bottom) showed two oxidation events in the forward scan from around 1.6 V onward. The corresponding O_2 trace (Fig. 3.14a, middle) showed that dioxygen evolution follows the recorded current profile, which suggests that both oxidation waves correspond to an oxygen evolution reaction. The formation of dioxygen therefore must be feasible for Fe(Hbbpya) in combination with a PG working electrode starting around 1.6 V, whereas with a gold working electrode this is not the case until about 1.9 V (Fig. 3.14b, middle). In case of Fe(Mebbpya) in combination with a gold working electrode an earlier onset of oxygen evolution was found at about 1.8 V according to OLEMS. Based on the current displayed, the onset may actually be a little earlier. Similar to Fe(Mebbpya) no CO_2 formation was observed at a gold electrode in presence of Fe(Hbbpya) (Fig. 3.14b, top), showing that no significant ligand degradation takes place.

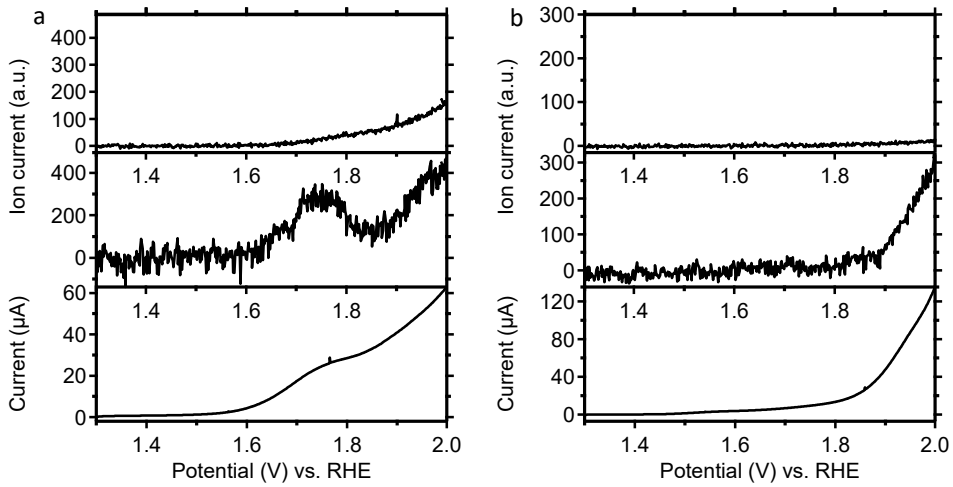

Figure 3.14. Cyclic voltammetry in combination with OLEMS of 0.5 mM Fe(Hbbpya) in 0.1 M Na_2SO_4 at a scan rate of 1 mV/s, using a PG (a) and a gold (b) working electrode. Depicted are the *m/z* traces of CO_2 (top), O_2 (middle) and the corresponding current (bottom). For the sake of clarity only the forward sweep of the 2nd scan is shown. The figure was adapted from reference [4].

3.2.4 Determination of the faradaic efficiency

The OLEMS results obtained with Fe(Hbbpya) at PG (Fig. 3.14a, middle) showed O_2 evolution with an onset both around 1.6 V and 1.9 V. As the OLEMS technique is qualitative and not easily calibrated, it does not give a quantitative description of the product formation. In order to determine whether the amount of O_2 that was detected at a low overpotential is actually significant, rotating ring disk electrode (RRDE) experiments were performed. Due to the rotation of the electrode, the electrolyte flows from the disk where water oxidation occurs to the ring where dioxygen is reduced and can be quantified. Since both the catalyst and dioxygen are diffusive species, partially oxidized catalytic species and dioxygen can both be reduced on the ring. As a result, the current at the disk electrode comprises three parts: current caused by catalytic water oxidation, reversible oxidation of the catalyst and losses from irreversible side reactions such as CO_2 formation. The contributions from reversible oxidation of dissolved complex in solution and formation of dioxygen were therefore disentangled by two separate RRDE experiments.

The sum of the current caused by oxidation of the complex and dioxygen formation was determined by using a Pt ring electrode set to 0.5 V vs. RHE in combination with a PG disk electrode (Fig. 3.15a). The current at the Pt ring was

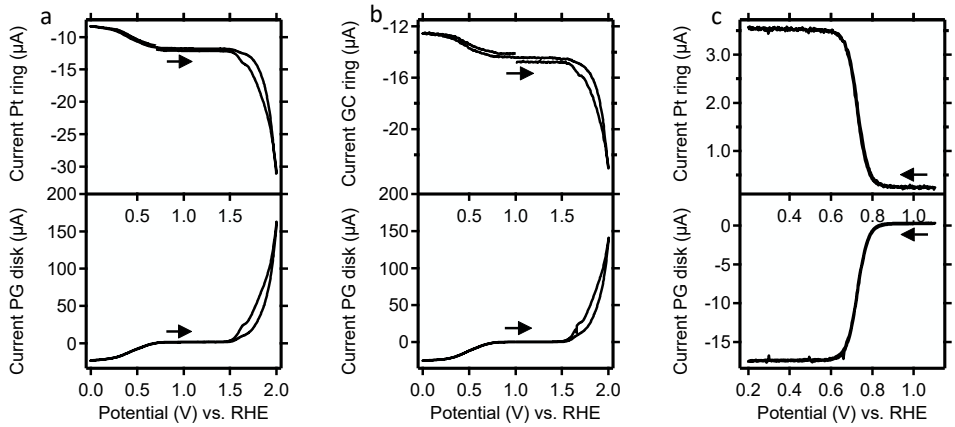

Figure 3.15. Results of a RRDE experiment in 0.1 M Na_2SO_4 at a scan rate of 10 mV/s and at a rotation speed of 800 RPM with (a) 0.5 mM Fe(Hbbpya), using a PG disk electrode and a Pt ring electrode, keeping the potential at the ring electrode at a constant value of 0.5 V vs. RHE, (b) 0.5 mM Fe(Hbbpya), using a PG disk electrode and a GC ring electrode, keeping the potential at the ring electrode at a constant value of 0.5 V vs. RHE and (c) 0.5 mM $K_3[Fe(CN)_6]$, using a PG disk electrode and a Pt ring electrode, keeping the potential at the ring electrode at a constant value of 1.2 V vs. RHE. The arrows in the figure indicate the direction of the scan.

measured to be 9.3% of the current at the PG disk at 1.75 V vs. RHE and 12.5% of the current at the PG disk at 2.0 V vs. RHE. The amount of current caused only by reversible oxidation of the complex was then quantified separately in a second experiment using a GC ring electrode instead of Pt as the GC ring electrode does not reduce dioxygen at a potential of 0.5 V vs. RHE (Fig. 3.15b). With the GC ring electrode the amount of current at the ring electrode caused by reduction of oxidized complex was found to be 4.5% of the current at the PG disk at 1.75 V vs. RHE and 6.3% of the current at the PG disk at 2.0 V vs. RHE. From this experiment it follows that the remaining 4.8% of the current at the PG disk at 1.75 V and 6.2% of the current at the PG disk at 2.0 V vs. RHE are the result of dioxygen reduction at the Pt ring.

To determine the maximum collection efficiency of dioxygen, another RRDE experiment with a Pt disk and a Pt ring in the absence of Fe(Hbbpya) was performed. However, the poor solubility of dioxygen in water resulted in the formation of bubbles at the surface of the Pt disk electrode which prevented an accurate determination of the collection efficiency of O_2. Instead the ferrocyanide/ferricyanide redox couple of $K_3[Fe(CN)_6]$ was used, in combination with a PG disk electrode and Pt ring electrode, to determine the collection efficiency of the RRDE setup at 19% (Fig. 3.15c).

For Fe(Hbbpya) the following contributions to the current were found. At 1.75 V 26% of the current is due to dioxygen formation and 23% is due to reversible losses. The remaining 51% is then attributed to irreversible losses. At 2.0 V 32% of current is due to dioxygen formation, 33% due to reversible losses and 35% due to irreversible losses. The Faradaic efficiencies of dioxygen formation found for Fe(Hbbpya) are largely underestimated for three reasons. First, due to rotation, the transient time of catalytic species over the disk is limited and may be too short to complete a catalytic cycle, which results in a considerable amount of partially oxidized species that are reduced back at the ring. At a stationary electrode such species may complete the catalytic cycle to produce dioxygen. The attempts to further reduce the rotation speed and thereby increase the transient time of catalytic species over the disk resulted in a delayed response on the ring and were abandoned. Second, due to the low solubility of O_2 in water and consequent formation of bubbles that bypass the ring undetected, the collection efficiency of dioxygen on the ring can be significantly lower than that of other species, such as ferricyanide, which was used to determine the collection efficiency of the setup. Third, it was recently demonstrated in our group that there may be a significant

difference in collection efficiency between outer sphere electron transfer processes, such as in ferricyanide, and multielectron multistep catalytic reactions, such as the water oxidation and oxygen reduction reaction (ORR). In case of ORR catalysed by $[Cu(tmpa)(L)]^{2+}$ (tmpa = tris(2-pyridylmethyl)amine, L = solvent) a collection efficiency of 12% for H_2O_2 at the Pt ring was found, instead of the expected value of 21%.[21] Therefore the values calculated for our system are most likely underestimated when compared to the ones obtained with the ferrocyanide/ferricyanide redox couple. In a separate RRDE experiment using a Pt disk electrode and a Pt ring electrode a faradaic efficiency for dioxygen evolution of only 68% at 1.7 V was found. As a result, the turnover frequencies mentioned below for water oxidation catalysed by Fe(Hbbpya) should be considered as conservative estimates.

For the determination of the TOF of Fe(Hbbpya) at different overpotentials equation 1 was used in combination with the Faradaic efficiency obtained from the RRDE experiments. In the equation, ν is the scan rate of the experiment, i_p is the peak current of the oxidation event at 1.0 V (cf. Fig. 3.6a), while i_{cat} is the catalytic current at the potential for which the TOF is determined. Additional details about the calculation of the TOFs are available in Appendix A.

$$TOF = 0.4848 \cdot \nu \left(\frac{i_{cat}}{i_p}\right)^2 \quad (1)$$

The results show that the TOF increases as the applied potential increases. At 1.75 V a TOF of 0.12 s^{-1} was found for Fe(Hbbpya) which increases to 1.2 s^{-1} at 2.0 V. This demonstrates that electron-transfer kinetics remain rate limiting until at least 2.0 V vs. RHE.

In case of Fe(Mebbpya) the determination of the faradaic efficiency could not be performed in the same way as for Fe(Hbbpya). During all the RRDE experiments bubbles were formed at the surface of the disk electrode due to the poor solubility of dioxygen in water, which prevented an accurate calculation of the collection efficiency. In contrast to Fe(Hbbpya), which is believed to adhere to graphitic electrodes *via* stacking interactions during catalysis,[4] Fe(Mebbpya) does not, which further decreases the retention time of the catalytic species on the disk. Consequently, Fe(Hbbpya) can turnover to produce dioxygen before the catalyst arrives at the ring, whereas this appeared to be less the case for the Fe(Mebbpya) complex. Therefore no faradaic efficiency could be calculated for Fe(Mebbpya).

Concerning the catalytic performance of Fe(Hbbpya), a comparison with data from literature is complicated by the fact that the majority of kinetic studies has been carried out in the presence of chemical oxidants rather than by electrochemical means, which leads to a poorly defined overpotential for those cases. However, the rates determined for Fe(Hbbpya) with graphitic working electrodes compare favourably to values reported in literature as most iron-based catalysts have been reported to exhibit TOFs of the order of 0.1 s^{-1} or lower in water. Typical examples range from 0.012 s^{-1} reported by Akermark *et al.* for $[Fe^{III,III}_2(H_2L)(\mu\text{-OMe})(OAc)]^+$ (H_5L = 2,2′-(2-hydroxy-5-methyl-1,3-phenylene)bis(1H-benzo[d]imidazole-4-carboxylic acid) to 0.23 s^{-1} for α-$[Fe(mcp)(OTf)_2]$ (mcp = *N*,*N*′-dimethyl-*N*,*N*′-bis(pyridin-2-ylmethyl)-cyclohexane-1,2-diamine) reported by Costas *et al.*[22-23] Some notable exceptions are represented by $[Fe(TAML)H_2O]^-$ (TAML = tetra-amido macrocyclic ligand) by Collins *et al.* and complex **5** (Fig. 3.1) by Thummel *et al.* for which initial rates of 1.3 s^{-1} and 2.2 s^{-1}, respectively, were found in the presence of excess CAN[24-25] and the pentanuclear iron catalyst $[Fe^{II}_4Fe^{III}(\mu_3\text{-O})(\mu\text{-L})_6]^{3+}$ (LH = 3,5-bis(2-pyridyl)pyrazole) developed by Masaoka *et al.*, which has been reported to have a remarkable turnover frequency of 1900 s^{-1}. In addition, it is also important to note that Fe(Hbbpya) shows a significantly earlier onset for OER by approximately 0.2 V in comparison to a series of Fe(cyclam) (cyclam = 1,4,8,11-tetraazacyclotetradecane) complexes that were reported earlier under identical reaction conditions, also using PG working electrodes.[26]

3.2.5 Determination of the rate orders for Fe(Mebbpya) and Fe(Hbbpya)

In order to ascertain the catalytic species potentially involved in the catalytic cycle, the rate order in [Fe] was determined. The effect of changes in concentration on the catalytic activity was evaluated by performing electrochemical experiments at different concentrations of Fe(Hbbpya) and Fe(Mebbpya) in a range between 1.2 mM and 0.1 mM. For the calculation of the rate order the logarithmic values of the catalytic current i_{cat} were plotted versus the logarithm of the concentrations. The values of i_{cat} were calculated by subtracting the blank current from the catalytic current at 2.0 V. In case of Fe(Hbbpya) in regimes of concentrations higher than 0.4 mM additional redox events were observed below 0.5 V. The observed behaviour may be related to a π-π stacking interaction between the aromatic systems of the Hbbpya ligands and the electrode surface, as an effect of the high concentration of complex in

solution. Instead, at concentrations lower than 0.4 mM only one oxidation and one reduction waves were visible (Fig. 3.16a), as expected from the second scan of a cyclic voltammogram of the complex (cf. Fig. 3.6a). Therefore, the rate order was calculated from the values of catalytic current obtained in a low concentration regime, where no π-π stacking effects were observed between catalytic species. In this regime a value of 0.1 was obtained (Fig. 3.16b). As observed in Fig. 3.16a the catalytic currents do not show a major change as a function of catalyst concentration, with the obtained rate order value close to zero-order. This is in line with a description wherein the Hbbpya complex is π-stacked onto the carbon surface to achieve a catalytic species. The catalytic rate in this case mostly depends on the electrode surface area rather than on the concentration of the catalyst.

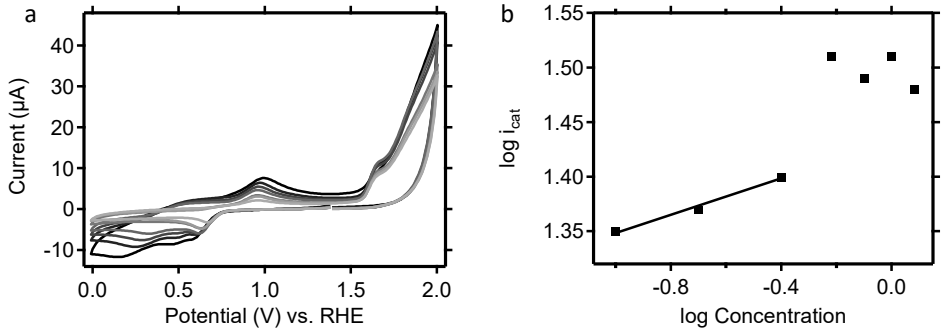

Figure 3.16. (a) Results of CV experiments of 0.5 mM Fe(Hbbpya) in 0.1 M Na_2SO_4, using a GC working electrode, at a scan rate of 100 mV/s. Displayed are the second scans of each CV recorded at concentrations varying from 1.2 mM to 0.1 mM, following the grey scale (1.2, 1.0, 0.8, 0.6, 0.4, 0.2 and 0.1 mM). (b) Displayed is the logarithm of i_{cat} vs. the logarithm of the values of concentration.

At concentrations higher than 0.6 mM additional redox events were observed for Fe(Mebbpya) as well (Fig. 3.17a), though less pronounced than for Fe(Hbbpya), showing a homogeneous behaviour. Moreover the catalytic currents show a major change as a function of catalyst concentration. The rate order for the water oxidation reaction was calculated from the entire set of data and a value of 0.6 was found (Fig. 3.17b). The rate order in [Fe] of 0.6 for Fe(Mebbpya) suggests that the active species responsible for catalysis corresponds to the monomeric form.[27]

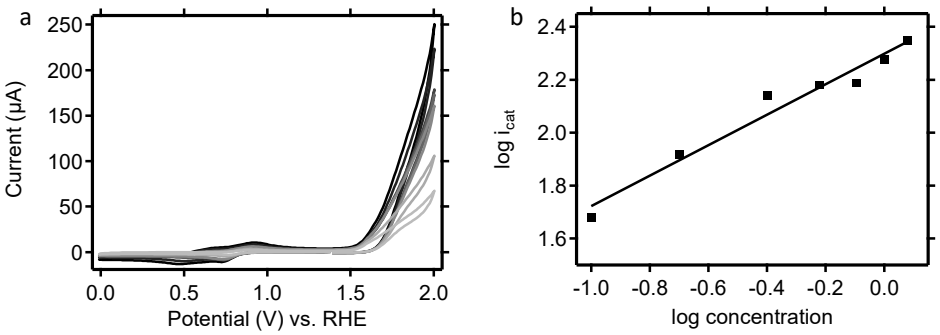

Figure 3.17. (a) Results of CV experiments of 0.5 mM Fe(Mebbpya) in 0.1 M Na_2SO_4, using a GC working electrode, at a scan rate of 100 mV/s. Displayed are the second scans of each CV recorded at concentrations varying from 1.2 mM to 0.1 mM, following the grey scale (1.2, 1.0, 0.8, 0.6, 0.4, 0.2 and 0.1 mM). (b) Displayed is the logarithm of i_{cat} vs. the logarithm of the values of concentration.

3.2.6 Kinetic isotope effect studies of Fe(Mebbpya) and Fe(Hbbpya)

The results obtained from the spectroelectrochemical experiments together with the values of the rate orders suggest that for both complexes the monomeric form is likely to be the active species responsible for catalysis. Monomeric species often react *via* a water nucleophilic attack mechanism.[5] When an O−H bond is broken during the rate-determining step of a reaction a kinetic isotope effect is expected. Kinetic isotope effect measurements were performed for both Fe(Hbbpya) and Fe(Mebbpya) in buffered water and deuterium oxide solutions. Cyclic voltammograms were measured in 10 mM acetate buffer (pH 4) solutions, in which both complexes are soluble (Fig. 3.18). The presence of the acetate

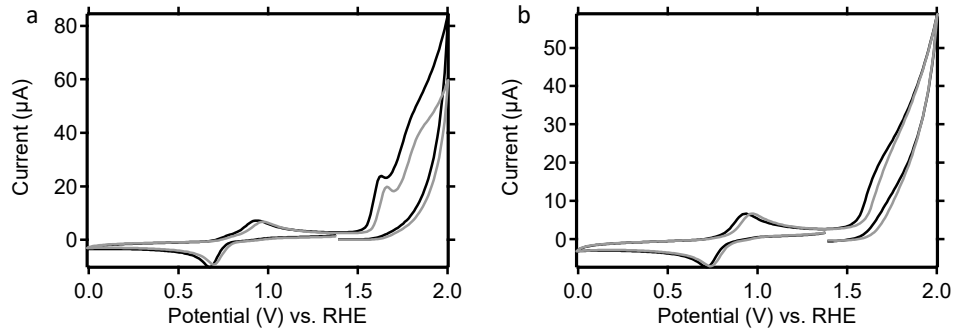

Figure 3.18. (a) Results of CV experiments of (a) Fe(Hbbpya) (0.5 mM) and (b) Fe(Mebbpya) (0.5 mM) performed with a GC working electrode at a scan rate of 100 mV/s. The CVs were measured in 10 mM acetate buffer (pH 4) with 0.1 M Na_2SO_4 to maintain the ionic strength. The figure displays the first scans of the experiments performed in water (black) and in deuterium oxide (grey).

buffer ensures that the pH/pD of both the H_2O and D_2O solutions is identical and that the corresponding activities can be directly compared. Interestingly, in the presence of acetate in the electrolyte only a single oxidation wave was observed for both Fe(Mebbpya) and Fe(Hbbpya). This may be due to coordination of acetate at the apical position, causing the dimeric structure to break. However, further research needs to be performed to corroborate this hypothesis.

Equation 2, wherein i_p is the peak current of the oxidation event at 0.9 V and i_{cat} the catalytic current, was used to determine the KIE values. Herein, i_{cat} was calculated by subtracting the blank current from the catalytic current at 2.0 V. For both complexes the data from three scans of one set of experiments conducted in water and deuterium oxide were averaged and the standard deviations were calculated.

$$KIE = \frac{k_{obs,H}}{k_{obs,D}} = \frac{\left(i_{cat}/i_p\right)^2_{H_2O}}{\left(i_{cat}/i_p\right)^2_{D_2O}} \quad (2)$$

In case of Fe(Hbbpya) a KIE value of 1.6 ± 0.1 was obtained. When the O−H bond of a water molecule is broken during the rate-determining step of the reaction a kinetic isotope effect is expected, with a lower reaction rate in presence of deuterium oxide, leading to a KIE > 1. The KIE value of 1.6 obtained with Fe(Hbbpya) suggests that a proton is transferred during the rate-determining step. Parent *et al.* reported a KIE of 2.6 ± 0.7 for the dinuclear complex **2** (Fig. 3.1)[1] and similar values of KIE were previously assigned to the rate-determining O−O bond formation step *via* a water nucleophilic attack.[5,28] With these results at hand we assume that a water nucleophilic attack mechanism most likely takes place, with O−O bond formation as part of the rate-determining step.

For complex Fe(Mebbpya) a KIE value of 0.9 ± 0.1 was observed. Given the structure of the complex the methylated amine cannot act as proton shuttle to activate a water molecule. As a consequence the breaking of the O−H bond is expected to be more difficult and therefore a larger KIE value should have been found if the same mechanism were to take place. This is in contrast with the obtained value of KIE of 0.9, which suggests that a proton transfer does not occur and therefore that a different rds is involved. A similar KIE value of 0.85 ± 0.04 was reported by Parent *et al.* for complex **1** (Fig. 3.1), which precludes a protonation as the rds.[1] This unusual value was previously observed for water

oxidation catalysts when the oxidant was involved in deprotonation[29] or the rds followed a pre-equilibrium.[28]

3.2.7 Proposed mechanisms for Fe(Mebbpya) and Fe(Hbbpya)

Based on the discussed results a mechanism for the water oxidation reaction catalysed by Fe(Hbbpya) and Fe(Mebbpya) is proposed. The absorption band at 350 nm observed in the UV-Vis spectra indicates that the starting state for both complexes in solution corresponds to a μ-oxo dimer. The dimeric structure undergoes a structural change during catalysis, as shown by the electrochemical and spectroelectrochemical evidence, generating a monomeric structure, which was assigned as the active species responsible for catalysis. Over time the dimeric structure is restored, which indicates that an equilibrium between the monomer and dimer forms is present. However, the different values of rate order and KIE suggest that the two catalysts react *via* different mechanisms.

In case of Fe(Hbbpya) the KIE value of 1.6 suggests that a proton is transferred during the rate-determining step. We assume that a water nucleophilic attack mechanism takes place, where an $Fe^{V}(O)$ intermediate undergoes the attack of a water molecule, with the breaking of the O−H bond and the formation of the O−O bond both occurring in the rate-determining step. However, we cannot rule out that the rate-determining step involves a proton-coupled electron transfer process that is not related to the O−O bond formation.

On the other hand the KIE value of 0.9 obtained for Fe(Mebbpya) precludes a protonation as the rds. In this case an electron transfer (ET) process may be involved or a bimolecular pathway may be followed, where the cooperation of two $Fe^{V}(O)$ intermediates leads to an intermolecular O−O bond formation.

Furthermore our observations suggest that the two catalysts may operate in different phases. Fe(Hbbpya) showed the tendency to adsorb on the electrode surface, whereas Fe(Mebbpya) showed a more homogeneous behaviour.

3.3 Conclusions

The Fe(Hbbpya) and Fe(Mebbpya) complexes proved to be molecular active electrocatalysts for the water oxidation reaction. When comparing the two catalysts, a similar catalytic activity and onset for the water oxidation reaction were found, although the results in case of Fe(Hbbpya) strongly depend on the electrode material. The dimeric and monomeric species are in both cases in

equilibrium with each other. The dimeric forms undergo a structural change once exposed to high potentials (2.0 V), presumably generating a monomeric form as the active species, which suggests that the dimeric forms act as mere pre-catalysts. Dimerization pathways were identified and a WNA rate-determining step was proposed for Fe(Hbbpya). However, blocking the proton shuttling capacities of the Hbbpya ligand by introduction of a methyl group did not halt catalysis. Instead, this structural change leads to a different mechanism of action, in which a different step appears to be rate-determining.

3.4 Experimental

3.4.1 Materials and instrumentation

All reagents and solvents were purchased from Sigma-Aldrich or VWR. The syntheses of the ligands and the iron complexes were carried out using standard Schlenk-line techniques.[4] 2,2'-Bipyridine mono N-oxide, 6-amino-2,2'-bipyridine and N,N-bis(2,2'-bipyrid-6-yl)amine were synthesized according to literature procedures.[30-33] The iron complex Fe(Hbbpya) was synthesized according to a reported procedure.[4] Solvents were degassed according to standard freeze-pump-thaw protocols. Mass spectra were measured on a Thermo Scientific MSQ Plus ESI spectrometer. NMR spectra were recorded on a Bruker 300 DPX spectrometer. UV-vis spectra were recorded on a Varian Cary 50 Scan spectrophotometer. Elemental analysis was performed by Mikroanalytisches Laboratorium Kolbe in Germany.

3.4.2 Electrochemical experiments

The electrochemical experiments were performed in custom-made single-compartment glass cells, using a three-electrode setup with the working electrode in hanging meniscus configuration. The data were recorded either on Ivium potentiostats, operated by IviumSoft software, or on Autolab PGstat10 potentiostats operated by NOVA 2.1.2 software. The working electrodes used in the experiments were a glassy-carbon (GC) rod, a pyrolytic graphite (PG) disk, a gold disk, an indium tin oxide plate (ITO) and a boron-doped-diamond (BDD) disk. The geometric surface areas of the working electrodes are 0.07 cm^2 (GC), 0.20 cm^2 (PG), 0.18 cm^2 (gold), 0.7 cm^2 (ITO), and 0.79 cm^2 (BDD). A gold wire was used as counter electrode and the reference electrode was a reversible hydrogen

electrode (RHE) made of a platinum mesh in a H_2-saturated electrolyte solution at the same pH as the electrolyte solution inside the cell. The reference electrode and the cell were connected *via* a Luggin capillary.

The GC electrode was pretreated before each experiment by polishing the electrode surface with alumina suspensions (1.0 µm followed by 0.3 µm and 0.05 µm). The PG electrode was prepared by polishing the electrode surface with sandpaper. For both the GC and the PG electrodes the polishing was followed by removing the excess debris by sonicating the electrode in Milli-Q water for 10 minutes. The gold electrode was prepared by oxidizing the surface at 10 V for 30 s in a 0.1 M H_2SO_4 solution, followed by stripping of the gold oxide layer in a 6 M HCl solution for 20 s. Subsequently, the electrode was electropolished by scanning 200 cycles between 0.0 and 1.75 V vs. RHE at 1 V/s in a 0.1 M $HClO_4$ electrolyte solution. For the experiments with an ITO working electrode, a small slice of ITO covered glass (ca. 0.5·1.5 cm) was used. While the gold and PG working electrodes were used in hanging meniscus configuration, the ITO electrode was partially submerged in the electrolyte solution. The BDD electrode was prepared by sonication for 5 minutes in Milli-Q water. Subsequently, the electrode was electropolished by scanning 200 cycles between -1.0 and 2.25 V vs. RHE at 1 V/s in a 0.1 M HNO_3 solution.

All glassware used in electrochemical measurements was routinely cleaned of any organic contamination by cleaning it overnight in a 0.5 M H_2SO_4 solution containing 1 g/L $KMnO_4$. The metal particles were afterwards removed by cleaning the glassware for 30 minutes in Milli-Q grade water (>18.2 MΩ cm resistivity) containing a few droplets of concentrated H_2SO_4 and 35% H_2O_2. The glassware was then cleaned by threefold rinsing with Milli-Q grade water and boiling it three times in Milli-Q grade water. Prior to each experiment the glassware was boiled in Milli-Q grade water for at least 1 h. All electrolyte solutions were prepared in Milli-Q water using puriss p.a. grade chemicals purchased from Honeywell, Merck Suprapur® or Sigma-Aldrich. Before the measurements the electrolyte solution was bubbled with argon (Linde, Ar 5.0) for at least 20 minutes. During the measurements the cell was constantly kept under argon atmosphere with an argon flow over the solution. Due to slow dissolution of Fe(Hbbpya) in a 0.1 M Na_2SO_4 electrolyte solution, the complex was first dissolved in 5 mL Milli-Q water and subsequently added to the electrolyte solution, which concentration was adjusted to account for the desired dilution. All experiments were performed at catalyst concentrations of 0.5 mM for Fe(Hbbpya) and Fe(Mebbpya).

For the OLEMS measurements, the gasses formed at the working electrode were collected *via* a hydrophobic tip (KEL-F with a porous Teflon plug) placed in close proximity to the surface of the working electrode and analysed in a QMS 200 mass spectrometer.[16] In all OLEMS experiments discussed in this chapter the potential was cycled between 1.3 and 2.0 V at 1 mV/s for a total of three cycles.
EQCM experiments were performed in a 5 mL Teflon cell purchased from Autolab. The top part of the cell was modified to allow for electrochemical measurements under an inert atmosphere. Autolab EQCM electrodes with a surface area of 1.5 cm^2 consisting of a 200 nm gold layer deposited on a quartz crystal were used as working electrodes. A custom-made RHE reference electrode was used.[17]
RRDE experiments were performed in a large single-compartment glass cell with a Pine rotator, using Pt and GC ring electrodes and a PG disk electrode purchased from Pine. Before the measurement the ring and disk electrodes were polished with alumina suspensions (1.0, 0.3, and 0.05 µm) and the excess debris was removed by sonicating the electrodes in Milli-Q water for 10 minutes.

3.4.3 Spectroelectrochemical experiments

The spectroelectrochemical experiments were performed with the OTTLE cell purchased from Spectroelectrochemistry Reading, a spin-out company at the University of Reading. The OTTLE cell is composed of a gold mesh working electrode, a platinum mesh counter electrode and a silver wire as pseudo-reference electrode. The windows are made from CaF_2. The electrochemical experiments performed in the OTTLE cell were controlled with an Autolab PGstat10 potentiostat operated by NOVA 2.1.2 software. UV-vis spectra were recorded on a Varian Cary 50 Scan spectrophotometer. Before the measurements the electrolyte solution was bubbled with N_2 in order to accomplish zero oxygen. A syringe was used to fill the cell with a volume of 200 µL of the analyte solution. All OTTLE cell experiments were performed at catalyst concentrations of 1.0 mM for Fe(Hbbpya) and Fe(Mebbpya) in a 0.1 M Na_2SO_4 electrolyte solution. Due to the silver pseudo-reference electrode the values of potential can undergo a shift in potential at every scan. The potential values obtained versus the pseudo-reference were recalculated to the RHE reference scale by taking the $[Fe^{III}Fe^{II}]/[Fe^{III}Fe^{III}]$ oxidation of a regular CV experiment vs. RHE as reference (Fig. 3.19).

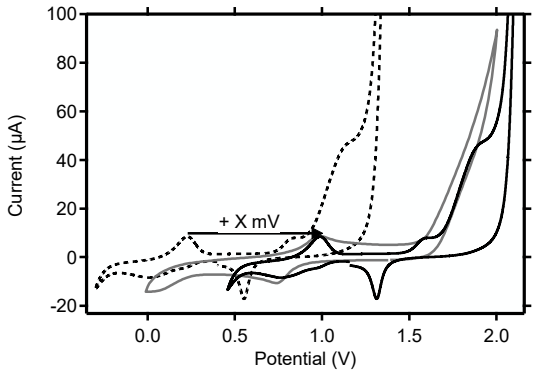

Figure 3.19. Conversion of the values of potential from a pseudo-reference electrode to the RHE reference electrode. Displayed are the 2nd scans of the cyclic voltammograms recorded in 0.1 M Na_2SO_4 with an OTTLE cell using a gold mesh working electrode vs. a silver pseudo-reference (black dashed line) and with a regular electrochemistry cell using a three-electrode setup with a GC working electrode vs. RHE (grey solid line). The cyclic voltammogram recorded with the OTTLE cell and plotted versus the corrected potential (vs. RHE) is displayed in the black solid line. The arrow indicates the potential shift in order to convert a pseudo-reference to a RHE reference.

Before performing the chronoamperometry experiments a regular cyclic voltammogram of the complexes was recorded with the OTTLE cell between 0.55 V and 2.25 V vs. RHE at a scan rate of 2 mV/s. The low scan rate allows for an accurate localization of the redox processes (Fig. 3.20). As the working electrode consists of a gold mesh, the gold reduction and gold oxidation peaks are observed at 1.3 V and around 1.6 V, respectively.

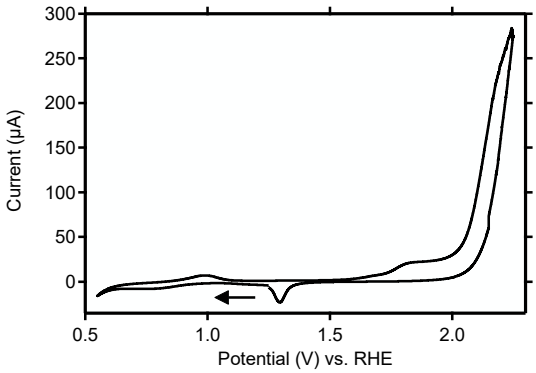

Figure 3.20. Cyclic voltammogram of 1.0 mM Fe(Hbbpya) in 0.1 M Na_2SO_4, recorded with the OTTLE cell. Displayed is the second scan recorded between 0.55 V and 2.25 V vs. RHE, starting at 1.25 V vs. RHE, at a scan rate of 2 mV/s. The arrow indicates the direction of the scan.

3.4.4 Synthesis of N,N-bis(2,2'-bipyrid-6-yl)methylamine, Mebbpya

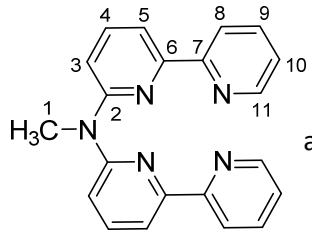

Hbbpya (402 mg, 1.24 mmol) and KOtBu (286 mg, 2.47 mmol) were dissolved in dry DMF (20 mL) under N_2 atmosphere. Iodomethane (154 µL, 2.47 mmol) was added dropwise and the mixture was stirred overnight in the dark by covering the flask with aluminum foil. Water (40 mL) and EtOAc (30 mL) were added to the reaction mixture and the aqueous layer was extracted with EtOAc (4·30 mL). The combined organic layers were dried over Na_2SO_4 and evaporated. The remaining orange oil product was dried under vacuum. Yield: 70 - 95 %. ^{1}H NMR (300 MHz, $CDCl_3$): δ = 8.69 (dq, ^3J=4.7 Hz, ^5J=0.9 Hz, 2H, H^{11}), 8.40 (dt, ^3J=8.0 Hz, ^5J=1.0 Hz, 2H, H^8), 8.05 (dt, ^3J=7.6 Hz, ^5J=0.7 Hz, 2H, H^5), 7.80 (tt, ^3J= 7.8 Hz, ^4J=1.8 Hz, 2H, H^9), 7.71 (tt, ^3J=8.3 Hz, 2H, H^4), 7.30 (m, 4H, H^3, H^{10}), 3.84 ppm (s, 3H, H^1). ^{13}C NMR ($CDCl_3$) δ = 157.2 (C^2), 156.4 (C^6), 154.4 (C^7), 149.2 (C^{11}), 138.2 (C^4), 137.0 (C^9), 123.7 (C^{10}), 121.2 (C^8), 114.6 (C^3), 114.1 (C^5), 36.1 (C^1) ppm. ESI-MS (MeOH) m/z Found: 340.2 $[M+H]^+$, 362.2 $[M+Na]^+$; calcd.: 340.2 $[M+H]^+$, 362.1 $[M+Na]^+$.

3.4.5 Synthesis of Fe(Mebbpya)

Fe(Mebbpya) was synthesized *via* the same procedure used for Fe(Hbbpya).[4] A solution of $Fe(OTf)_2$·5.5 H_2O (554 mg, 1.22 mmol) in degassed MeOH (30 mL) was added to a solution of Mebbpya (410 mg, 1.21 mmol) dissolved in degassed MeOH (20 mL). The deep red mixture was stirred for 30 hours under N_2. The solvent was then removed under vacuum and the crude product was dissolved in MeOH (2.0 mL) and crystallized by vapour diffusion with diethyl ether. The dark brown needle-shaped crystals obtained were collected by filtration, washed with diethyl ether and dried in air. Yield: 84 %. ^{1}H NMR (300 MHz, CD_3OD): δ = 18.04, 15.37, 8.55, 8.42, 8.11, 8.03, 7.60, 3.86 ppm. Elemental analysis calcd. (%) for $C_{46}H_{38}F_{12}Fe_2N_{10}O_{15}S_4$ (1438.78 g/mol): C 38.40, H 2.66, N 9.74; found: C 38.43, H 2.71, N 9.70. ESI-MS (H_2O) m/z Found: 318.2 $[Fe^{III}$(Mebbpya)-µ-O-(Mebbpya)Fe^{III}(OTf)$]^{3+}$, 440.2 $[Fe^{III}$(Mebbpya)$(CHO_2)]^{2+}$, 544.1 $[Fe^{III}$(Mebbpya)(OTf)$]^{2+}$, 340.0 $[$(Mebbpya)+H$]^+$; calcd.: 318.4 $[Fe^{III}$(Mebbpya)-µ-O-(Mebbpya)Fe^{III}(OTf)$]^{3+}$, 440.1 $[Fe^{III}$(Mebbpya)$(CHO_2)]^{2+}$, 544.0 $[Fe^{III}$(Mebbpya)(OTf)$]^{2+}$, 340.2 $[$(Mebbpya)+H$]^+$.

3.5 References

[1] Parent, A. R.; Nakazono, T.; Lin, S.; Utsunomiya, S.; Sakai, K., *Dalton Trans.* **2014,** *43*, 12501.

[2] Wickramasinghe, L. D.; Zhou, R.; Zong, R.; Vo, P.; Gagnon, K. J.; Thummel, R. P., *J. Am. Chem. Soc.* **2015,** *137*, 13260.

[3] Najafpour, M. M.; Moghaddam, A. N.; Sedigh, D. J.; Hołyńska, M., *Catal. Sci. Technol.* **2014,** *4*, 30.

[4] Kottrup, K. G.; D'Agostini, S.; van Langevelde, P. H.; Siegler, M. A.; Hetterscheid, D. G. H., *ACS Catal.* **2018,** *8*, 1052.

[5] Chen, Z.; Concepcion, J. J.; Hu, X.; Yang, W.; Hoertz, P. G.; Meyer, T. J., *Proc. Natl. Acad. Sci.* **2010,** *107*, 7225.

[6] Matheu, R.; Ertem, M. Z.; Benet-Buchholz, J.; Coronado, E.; Batista, V. S.; Sala, X.; Llobet, A., *J. Am. Chem. Soc.* **2015,** *137*, 10786.

[7] van Rixel, V. H. S. PhD thesis "Towards selective anticancer metallodrugs". Leiden University, **2017**.

[8] den Boer, D.; Hetterscheid, D. G. H.; Konovalov, A. I., Leiden University.

[9] Kottrup, K. PhD thesis "Iron complexes as electrocatalysts for the water oxidation reaction". Leiden University, **2018**.

[10] Bard, A. J.; Faulkner, L. R., *Electrochemical methods: fundamentals and applications*. 2nd ed.; John Wiley & Sons: New York, **2001**; p 286.

[11] Schley, N. D.; Blakemore, J. D.; Subbaiyan, N. K.; Incarvito, C. D.; D'Souza, F.; Crabtree, R. H.; Brudvig, G. W., *J. Am. Chem. Soc.* **2011,** *133*, 10473.

[12] van der Ham, C. J. M.; Işık, F.; Verhoeven, T. W. G. M.; Niemantsverdriet, J. W.; Hetterscheid, D. G. H., *Catal. Today* **2017,** *290*, 33.

[13] van Dijk, B.; Hofmann, J. P.; Hetterscheid, D. G. H., *Phys. Chem. Chem. Phys.* **2018,** *20*, 19625.

[14] Hetterscheid, D. G. H., *Chem. Commun.* **2017,** *53*, 10622.

[15] Sauerbrey, G., *Zeitschrift für Physik* **1959,** *155*, 206.

[16] Wonders, A. H.; Housmans, T. H. M.; Rosca, V.; Koper, M. T. M., *J. Appl. Electrochem.* **2006,** *36*, 1215.

[17] Abril, P.; del Río, M. P.; Tejel, C.; Verhoeven, T. W. G. M.; Niemantsverdriet, J. W. H.; Van der Ham, C. J. M.; Kottrup, K. G.; Hetterscheid, D. G. H., *ACS Catal.* **2016,** *6*, 7872.

[18] Fukuzumi, S.; Hong, D., *Eur. J. Inorg. Chem.* **2014,** *2014*, 645.

[19] Hintermair, U.; Sheehan, S. W.; Parent, A. R.; Ess, D. H.; Richens, D. T.; Vaccaro, P. H.; Brudvig, G. W.; Crabtree, R. H., *J. Am. Chem. Soc.* **2013,** *135*, 10837.

[20] Limburg, B.; Bouwman, E.; Bonnet, S., *Coord. Chem. Rev.* **2012,** *256*, 1451.

[21] Langerman, M.; Hetterscheid, D. G. H., *Angew. Chem. Int. Ed.* **2019,** *58*, 12974.

[22] Fillol, J. L.; Codola, Z.; Garcia-Bosch, I.; Gomez, L.; Pla, J. J.; Costas, M., *Nat. Chem.* **2011,** *3*, 807.

[23] Das, B.; Lee, B. L.; Karlsson, E. A.; Akermark, T.; Shatskiy, A.; Demeshko, S.; Liao, R. Z.; Laine, T. M.; Haukka, M.; Zeglio, E.; Abdel-Magied, A. F.; Siegbahn, P. E.; Meyer, F.; Karkas, M. D.; Johnston, E. V.; Nordlander, E.; Akermark, B., *Dalton Trans.* **2016,** *45*, 13289.

[24] Ellis, W. C.; McDaniel, N. D.; Bernhard, S.; Collins, T. J., *J. Am. Chem. Soc.* **2010,** *132*, 10990.

[25] Wickramasinghe, L. D.; Zhou, R.; Zong, R.; Vo, P.; Gagnon, K. J.; Thummel, R. P., *J. Am. Chem. Soc.* **2015,** *137*, 13260.

[26] Kottrup, K. G.; Hetterscheid, D. G., *Chem. Commun.* **2016,** *52*, 2643.

[27] Vallance, C., An Introduction to Chemical Kinetics. Morgan & Claypool Publishers: **2017**.

[28] Blakemore, J. D.; Schley, N. D.; Balcells, D.; Hull, J. F.; Olack, G. W.; Incarvito, C. D.; Eisenstein, O.; Brudvig, G. W.; Crabtree, R. H., *J. Am. Chem. Soc.* **2010,** *132*, 16017.

[29] Wasylenko, D. J.; Ganesamoorthy, C.; Henderson, M. A.; Berlinguette, C. P., *Inorg. Chem.* **2011,** *50*, 3662.

[30] Norrby, T., *Acta Chem. Scand.* **1998,** *52*, 77.

[31] Joachim Demnitz, F. W.; D'Heni, M. B., *Org. Prep. Proced. Int.* **1998,** *30*, 467.

[32] Yin, J.; Xiang, B.; Huffman, M. A.; Raab, C. E.; Davies, I. W., *J. Org. Chem.* **2007,** *72*, 4554.

[33] Zheng, S.; Reintjens, N. R. M.; Siegler, M. A.; Roubeau, O.; Bouwman, E.; Rudavskyi, A.; Havenith, R. W. A.; Bonnet, S., *Chem. Eur. J.* **2016,** *22*, 331